Abstract for 37th IWWWFB, Giardini Naxos, Italy - April 10-13, 2022

Decomposition of ship waves and time-frequency spectrograms

Hui Liang, Harrif Santo, Michael Si

Technology Centre for Offshore and Marine, Singapore (TCOMS), 118411, Singapore

E-mail: liang_hui@tcoms.sg

Highlights

- The viscous-ship-wave Green function [1] is applied to study wave patterns generated by a ship hull;
- The KHP approximation [2, 3] is conducted rendering a decomposition of transverse and divergent waves;
- Time-frequency spectrograms are analysed to study the amplitudes of transverse and divergent waves.

1 Green function and Hogner model

The ship-wave Green function represents the flow induced by a point singularity (source, sink, or dipole) with unit strength translating steadily along a straight path in calm water, and it is an essential building block to constructing the boundary integral equation to model free-surface flows by an advancing ship hull within the linear potential theory. As reported in [4], however, very short and steep divergent waves exist when both source and flow-field points are on the free surface. Moreover, the wave amplitude is unbounded as the flow-field point approaches the track of the source point. To eliminate these unphysical behaviours, fluid viscosity is accounted for as in [1]. Under the influence of fluid viscosity effects, and singular behaviour is eliminated, and steep short waves are severely damped out. This viscous-ship-wave Green function is then used as the fundamental solution to construct the boundary integral equation to model wave patterns by a ship hull.

A frame of reference $Oxyz$ translating with the ship at a constant speed U in the direction of the positive x-axis is defined with the Oxy plane coinciding with the undisturbed free surface and z-axis orienting positively upward. Following [1], the viscous-ship-wave Green function is

$$4\pi G = -1/r + 1/d + G^F, \quad \text{with } \{r, d\} = \sqrt{(x-\xi)^2 + (y-\eta)^2 + (z \mp \zeta)^2}, \tag{1}$$

where $\mathbf{x} \equiv (x, y, z)$ and $\boldsymbol{\xi} \equiv (\xi, \eta, \zeta)$ denote the flow-field point and source point, respectively, and G^F is the free-surface term in the form of a double Fourier integral. The free-surface term G^F can be decomposed into a non-oscillatory local-flow component G^L and a wave component G^W dominant in the far field, given by

$$G^L = \frac{2\kappa}{\pi}\mathrm{Im}\int_{-1}^{1} \mathrm{e}^Z E_1(Z)\mathrm{d}q, \quad \text{with } Z = -\mathrm{i}\kappa\sqrt{1-q^2}[-|x-\xi| + \mathrm{i}\sqrt{1-q^2}(z+\zeta) - \mathrm{i}q(y-\eta)], \tag{2}$$

$$G^W = 4H(\xi - x)\mathrm{Im}\int_{-\infty}^{\infty} \kappa \exp\left\{\kappa(1+q^2)(z+\zeta) + 4\epsilon\kappa(x-\xi)\frac{(1+q^2)^3}{1+2q^2} + \mathrm{i}\kappa\sqrt{1+q^2}[(x-\xi) - q(y-\eta)]\right\}\mathrm{d}q, \tag{3}$$

where $\mathrm{e}^u E_1(u)$ is the complex exponential-integral function, κ is defined as $\kappa = g/U^2$, and ϵ is a parameter associated with viscous effects defined as $\epsilon = g\nu/U^3$.

To model free-surface flows around a ship hull, the highly simple but realistic Hogner model [5] is adopted. The flow induced by an advancing ship hull is represented by a source distribution with strength n_ξ over the mean wetted hull surface

$$\phi(\mathbf{x}) = \iint_{\Sigma^H} n_\xi G(\mathbf{x}, \boldsymbol{\xi})\mathrm{d}S, \tag{4}$$

where Σ^H denotes the mean wetted hull surface, and n_ξ is the component in x-direction of the vector normal to the ship hull. Introducing polar coordinates $(x, y) = h(-\cos\gamma, \sin\gamma)$, where γ is measured from the negative x-axis, the potential induced by the ship hull in the far field ($h/L \gg 1$) is written in a Fourier-Kochin form [6]

$$\phi^W(\mathbf{x}) = \iint_{\Sigma^H} n_\xi G^W(\mathbf{x}, \boldsymbol{\xi})\mathrm{d}S = \frac{\kappa}{\pi}\mathrm{Im}\int_{-\infty}^{\infty} A(\mathbf{x}, q)\mathrm{e}^{\mathrm{i}\kappa h\psi(q,\gamma)}\mathrm{d}q, \tag{5}$$

where the Kochin function $A(\mathbf{x}, q)$ and phase function $\psi(q, \gamma)$ are written as:

$$A(\mathbf{x}, q) = \iint_{\Sigma^H} n_\xi \exp\left[\kappa(1+q^2)(z+\zeta) + 4\epsilon\kappa(x-\xi)\frac{(1+q^2)^3}{1+2q^2} + \mathrm{i}\kappa\sqrt{1+q^2}(\xi + q\eta)\right]\mathrm{d}S, \tag{6}$$

$$\psi(q, \gamma) = \sqrt{1+q^2}(\cos\gamma - q\sin\gamma). \tag{7}$$

2 Uniform KHP approximation

The uniform asymptotic approximation to the wavenumber integral (5) is considered. Unlike the classical CFU approximation [7] involving the Airy function and its derivative, the KHP approximation [2, 3] only involves elementary functions. Moreover, the KHP approximation is able to provide an explicit decomposition of transverse and divergent waves that exist inside the cusps of the wave pattern.

Within Kelvin's wedge $\gamma < \gamma_c \equiv 19°28'$, there are two stationary points requiring the vanishing of the first-order derivative of the phase function, i.e. $\psi'(q,\gamma) = 0$, and they are given by

$$q_\pm = (1 \pm Q)\cot\gamma/4, \quad \Rightarrow \quad \psi''_\pm \equiv \psi''(q_\pm,\gamma) = \mp\frac{4}{\sqrt{3}}\frac{Q\sin\gamma}{\sqrt{(1\pm Q)(1\mp Q/3)}}, \quad \text{with } Q = \sqrt{1-8\tan^2\gamma}. \tag{8}$$

At the cusp $\gamma = \gamma_c$, two stationary points coalesce $q_- = q_+ = q_c = 1/\sqrt{2}$, and both first- and second-order derivatives of the phase function are nil, e.g.: $\psi'(q_c,\gamma_c) = \psi''(q_c,\gamma_c) = 0$. The third- and fourth-order derivatives at q_c are

$$\psi'''_c \equiv \psi'''(q_c,\gamma_c) = -4\sqrt{6}/9, \quad \text{and} \quad \psi''''_c \equiv \psi''''(q_c,\gamma_c) = 8\sqrt{3}/9. \tag{9}$$

Outside Kelvin's wedge $\gamma > \gamma_c$, two stationary points turn to two complex saddle points which are a complex conjugate pair. By deforming the integration path, only the contribution of the saddle point at which the imaginary part of ψ'' is larger than zero matters, and the selected saddle point is

$$q_o = (1-\mathcal{Q})\cot\gamma/4, \quad \Rightarrow \quad \psi''_o \equiv \psi''(q_o,\gamma) = \frac{4}{\sqrt{3}}\frac{\mathcal{Q}\sin\gamma}{\sqrt{(1-\mathcal{Q})(1+\mathcal{Q}/3)}}, \quad \text{with } \mathcal{Q} = \mathrm{i}\sqrt{8\tan^2\gamma - 1}. \tag{10}$$

Based on [3], the approximation to wave pattern inside the cusp $\gamma \le \gamma_c$, combining ones due to Kelvin and Havelock, is written as

$$\phi^W(\mathbf{x}) \approx \frac{\kappa}{\pi}\mathrm{Im}\left[F_-^{KH}\mathrm{e}^{\mathrm{i}(\kappa h\psi_- + \pi/4)} + F_+^{KH}\mathrm{e}^{\mathrm{i}(\kappa h\psi_+ - \pi/4)}\right], \tag{11}$$

where the functions $F_\pm^{KH}$ are defined as

$$F_\pm^{KH} = (1-\mathrm{e}^{-u^{4/3}})\frac{\sqrt{2\pi}A_\pm}{\sqrt{\kappa h|\psi''_\pm|}} + \mathrm{e}^{-u^{4/3}}\frac{C_H^* A_c}{(\kappa h|\psi'''_c|)^{1/3}}\left[1 \mp \frac{\Gamma(2/3)}{\Gamma(1/3)}\left(\frac{A'_c}{A_c} - \frac{\psi''''_c}{6\psi'''_c}\right)\left(\frac{6}{\kappa h\psi'''_c}\right)^{1/3}\right], \tag{12}$$

with $C_H^* \equiv \Gamma(1/3)/6^{1/6} \approx 1.987334$, and $u = 3\kappa h|\psi_+ - \psi_-|/4$. Eq. (11) provides an explicit decomposition of the two systems of waves consisting of transverse waves and divergent waves associated with the first term and second term, respectively, in the square bracket of Eq. (11). At the cusp, there is a phase difference $\pi/2$ of transverse and divergent waves. The approximation to wave pattern outside the cusp $\gamma \ge \gamma_c$, which combines approximations due to Havelock and Peters, is written as

$$\phi^W(\mathbf{x}) \approx \frac{\kappa}{\pi}\mathrm{Im}\left[F_o^{HP}\mathrm{e}^{\mathrm{i}(\kappa h\psi_o + \pi/4)}\right], \tag{13}$$

where the function F_o^{HP} is defined as

$$F_o^{HP} = (1-\mathrm{e}^{-v^{4/3}})\frac{\sqrt{2\pi}A_o}{\sqrt{\kappa h\psi''_o}} + \mathrm{e}^{-v^{4/3}}\frac{(1-\mathrm{i})C_H^* A_c}{(\kappa h|\psi'''_c|)^{1/3}}\left[\mathrm{e}^{-2v/3} + \mathrm{i}\frac{\Gamma(2/3)}{\Gamma(1/3)}\left(\frac{A'_c}{A_c} - \frac{\psi''''_c}{6\psi'''_c}\right)\left(\frac{6}{\kappa h\psi'''_c}\right)^{1/3}\right], \tag{14}$$

with $v = 3\kappa h\,|\mathrm{Im}(\psi_o)|/2$.

3 Wave patterns

For illustrative purposes, wave patterns generated by a modified Wigley hull model are considered, and the geometry of the Wigely hull is defined as

$$y = \pm\frac{L}{10}[(1-X^2)(1-Z^2)(1+0.2X^2) + Z^2(1-Z^8)(1-X^2)^4], \quad \text{where } X = \frac{2x}{L} \text{ and } Z = \frac{10z}{L}, \tag{15}$$

with $-L/2 \le x \le L/2$ and $-L/10 \le z \le 0$. In Eq. (15), L denotes the length of Wigley hull, and the Froude number associated with ship's speed is defined as $F = U/\sqrt{gL}$. Fig. 1 exhibits contour plots of wave patterns generated by the modified Wigley hull at $F = 0.4$, 0.6, and 0.8, respectively. Wave patterns together with their decomposition into transverse and divergent waves inside the cusp are displayed in the left, middle, and right subplots, respectively. The white dashed line in the left subplot corresponds to the cusp. At $F = 0.4$, the amplitude of transverse waves is appreciably larger than that of divergent waves, whereas the tendency is reversed at $F = 0.8$. The amplitudes of two wave systems are comparable at $F = 0.6$. Therefore, divergent waves play an increasingly dominant role with the increasing ship's velocity. Moreover, short divergent waves disappear near the track under the joint influences of fluid viscosity effects and ship hull interference effects as expounded in [1] and [8], respectively.

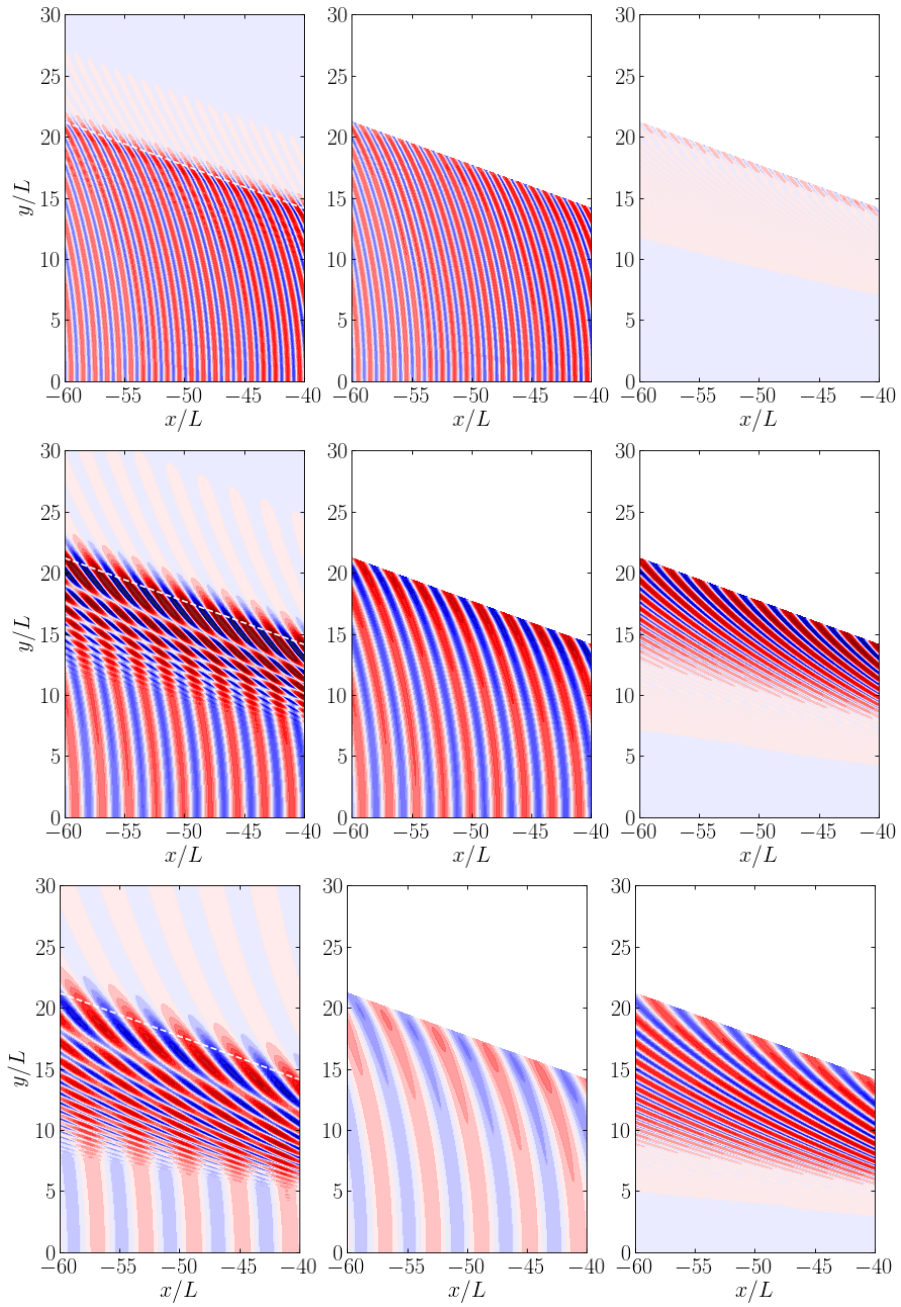

Figure 1: Wave patterns as well as decomposition into transverse waves and divergent waves for $F = 0.4$, 0.6, and 0.8 displayed in the top, middle, and bottom rows, respectively.

4 Time-frequency spectrogram

To further study the amplitudes of transverse and divergent waves inside Kelvin's wedge, the time-frequency spectrogram is studied. Based on the geometrical relation as in Fig. 2, we can obtain the frequencies of transverse waves and divergent waves measured at the sensor location [9]

$$\omega_{\pm} = \frac{g}{2\sqrt{2}U}\sqrt{\chi^2 \pm \chi\sqrt{\chi^2 - 8} + 4}, \quad \text{with } \chi \equiv Ut/y, \tag{16}$$

where y denotes the lateral distance between the sensor and ship's sailing line, and $t = 0$ corresponds to the time instant when the mid-ship is aligned with the sensor location. Eq. (16) gives rise to two branches plotted by the black line in Fig. 3. The lower and upper branches correspond to the frequencies of transverse waves and divergent waves at the sensor location. Two branches intersect at $Ut/y = 2\sqrt{2} = 1/\tan\gamma_c$ when the cusp of Kelvin's wake meets the sensor. With the time marching, the frequency of transverse waves is nearly constant, whereas that of divergent waves is steadily increasing. Besides, Fig. 3 shows time-frequency spectrograms of wave patterns generated by the modified Wigley hull at $y/L = 20$ for $F = 0.4$, 0.6, and 0.8 displayed in the left,

middle, and right subplots. The frequencies of transverse waves and divergent waves determined by spectrograms are in good agreement with the dispersion relation given by Eq. (16) as expected. At $F = 0.4$ as in the left subplot, divergent waves are inconsequential in consistency with top subplot in Fig. 1. With the increasing the Froude number, divergent waves are playing an increasingly important role. With the time marching, however, the amplitude of divergent waves at the sensor location diminishes. At the sensor location, the lateral distance from ship's sailing line keeps constant, whereas the inline distance is consistently increasing resulting in the decreasing of the polar angle γ. As elucidated in [1] and [8], divergent waves are largely damped out under influences of fluid viscosity and ship hull interference. Therefore, the sensor can only measure divergent waves over a period of time. Comparing three subplots, the duration of divergent waves is increasing with ship's speed.

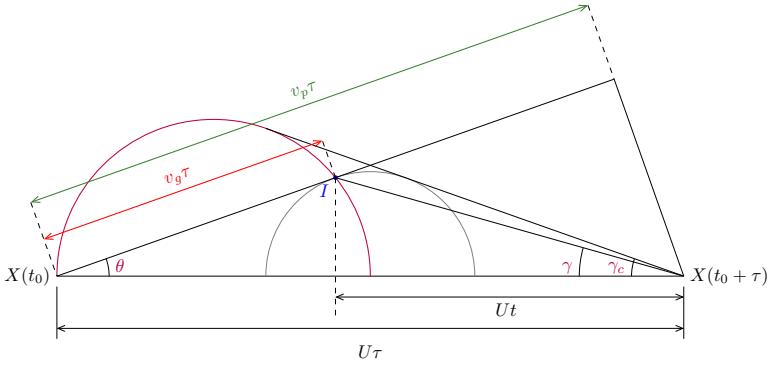

Figure 2: Ship wave dispersion. I is the sensor's position, $v_p = U\cos\theta$ the phase velocity, $v_g = 0.5U\cos\theta$ the group velocity, 'purple semi-circle' the boundary of energy at $t_0 + \tau$ generated by the ship at time instant t_0, $U\tau$ the inline distance sailed from t_0 to $t_0 + \tau$, and Ut the inline distance from the sensor to the ship at $t_0 + \tau$.

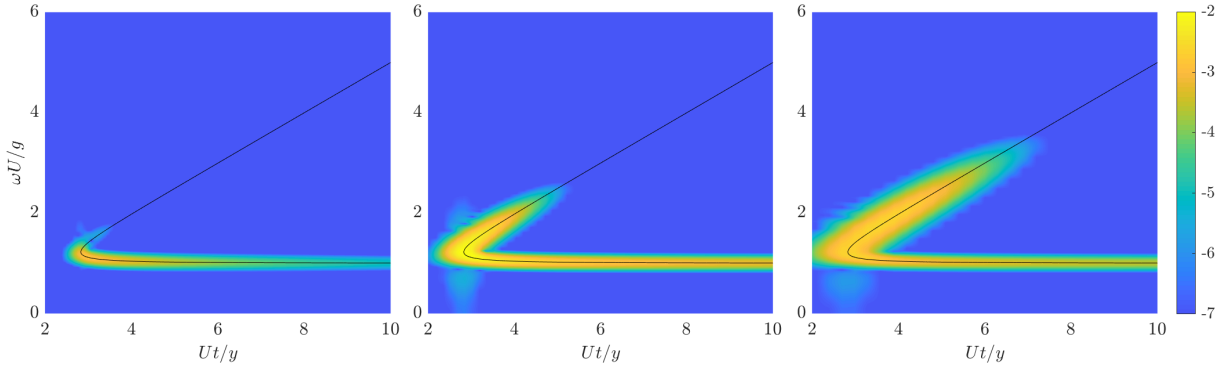

Figure 3: Spectrograms of ship-generated waves for $F = 0.4$ (left), 0.6 (middle), and 0.8 (right).

H.L. highly appreciates discussions with X.B. Chen at Bureau Veritas and R. Pethiyagoda at Queensland University of Technology. This research is supported by A*STAR under its RIE 2020 Industry Alignment Fund (A19F1a0104).

References

[1] H. Liang, & X. B. Chen, Viscous effects on the fundamental solution to ship waves. *J. Fluid. Mech.*, 879: 744–774, 2019.

[2] H. Wu, J. He, Y. Zhu, & F. Noblesse, The Kelvin–Havelock–Peters farfield approximation to ship waves. *Eur. J. Mech. (B/Fluids)*, 70: 93–101, 2018.

[3] H. Liang, H. Wu, J. He, & F. Noblesse, Kelvin–Havelock–Peters approximations to a classical generic wave integral. *Appl. Math. Model.*, 77: 950–962, 2020.

[4] F. Ursell, On Kelvin's ship-wave pattern. *J. Fluid. Mech.*, 8: 418–431, 1960.

[5] E. Hogner, Contributions to the theory of ship waves. *Ark. Mat. Astr. Fys.*, 17: 1–50, 1923.

[6] H. Wu, J. He, H. Liang, & F. Noblesse, Influence of Froude number and submergence depth on wave patterns. *Eur. J. Mech. (B/Fluids)*, 75: 258–270, 2019.

[7] C. Chester, B. Friedman, & F. Ursell, An extension of the method of steepest descents. *Math. Proc. Camb. Phil. Soc.*, 53: 599-611, 1959.

[8] H. Wu, J. Wu, J. He, R. Zhu, C. J. Yang, & F. Noblesse, Wave profile along a ship hull, short farfield waves, and broad inner Kelvin wake sans divergent waves. *Phys. Fluids*, 31: 047102, 2019.

[9] R. Pethiyagoda, S. W. McCue, & T. J. Moroney, Spectrograms of ship wakes: identifying linear and nonlinear wave signals. *J. Fluid. Mech.*, 811: 189–209, 2017.